iScience

Article

Enhanced differentiation of neural progenitor cells in Alzheimer's disease into vulnerable immature neurons

Graphical abstract

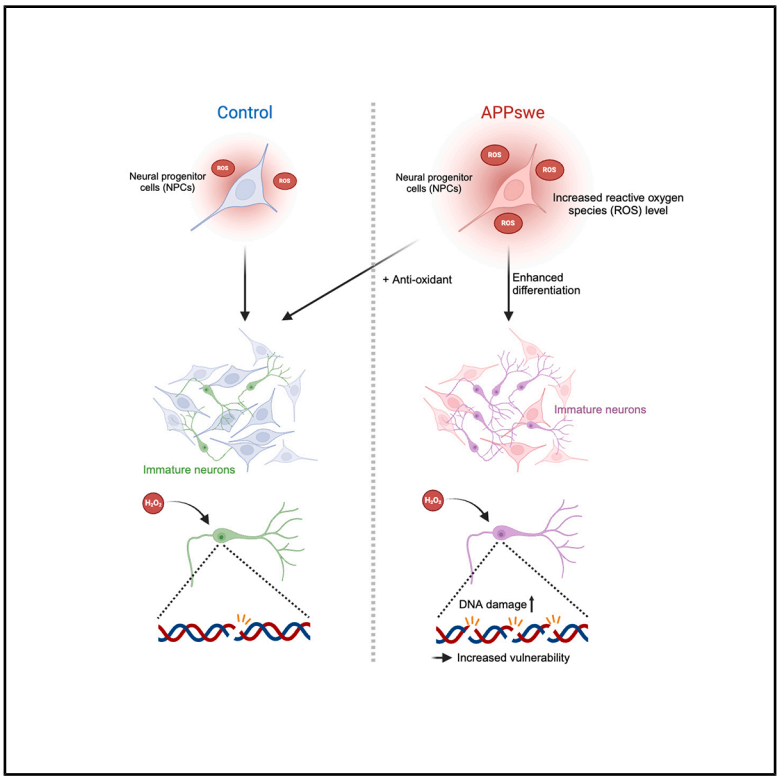

Highlights

- APPswe organoids show increased neural activity and early differentiation
- Enhanced ROS levels are necessary but insufficient to accelerate differentiation
- Transcriptome analysis of APPswe NPCs shows gene expression shift to differentiation
- Premature neural cells with APPswe exhibit increased vulnerability to toxicity

Authors

Joonho Cho, Simsung Bae, Juyeong Jeon, ..., Alexi Nott, Fan Gao, Jinsoo Seo

Correspondence

jseo@yonsei.ac.kr

In brief

Molecular biology; Neuroscience; Cell biology

Cho et al., 2025, iScience *28*, 112446
May 16, 2025
https://doi.org/10.1016/j.isci.2025.112446

CellPress

iScience

CellPress
OPEN ACCESS

Article

Enhanced differentiation of neural progenitor cells in Alzheimer's disease into vulnerable immature neurons

Joonho Cho,[1] Simsung Bae,[1] Juyeong Jeon,[1] Janis Transfeld,[3,4] Changyeob Lee,[1] Alexi Nott,[3,4] Fan Gao,[5] and Jinsoo Seo[1,2,6,7,*]

[1]Department of Brain Sciences, DGIST, Daegu 42988, South Korea
[2]Center for Synapse Diversity and Specificity, DGIST, Daegu 42988, South Korea
[3]UK Dementia Research Institute at Imperial College London, London, UK
[4]Department of Brain Sciences, Imperial College London, London, UK
[5]Bioinformatics Resource Center, Beckman Institute of Caltech, Pasadena, CA 91125, USA
[6]Department of Systems Biology, College of Life Science and Biotechnology, Yonsei University, Seoul 03722, South Korea
[7]Lead contact
*Correspondence: jseo@yonsei.ac.kr
https://doi.org/10.1016/j.isci.2025.112446

SUMMARY

Focusing on the early stages of Alzheimer's disease (AD) holds great promise. However, the specific events in neural cells preceding AD onset remain elusive. To address this, we utilized human-induced pluripotent stem cells carrying APPswe mutation to explore the initial changes associated with AD progression. We observed enhanced neural activity and early neuronal differentiation in APPswe cerebral organoids cultured for one month. This phenomenon was also evident when neural progenitor cells (NPCs) were differentiated into neurons. Furthermore, transcriptomic analyses of NPCs and neurons confirmed altered expression of neurogenesis-related genes in APPswe NPCs. We also found that the upregulation of reactive oxygen species (ROS) is crucial for early neuronal differentiation in these cells. In addition, APPswe neurons remained immature after initial differentiation with increased susceptibility to toxicity, providing valuable insights into the premature exit from the neural progenitor state and the increased vulnerability of neural cells in AD.

INTRODUCTION

Numerous clinical trials aimed at eliminating amyloid-beta (Aβ), a key pathological feature of Alzheimer's disease (AD), have yet to yield significant improvements in cognitive function. A promising approach is early-stage disease intervention, based on the hypothesis that intervening during AD's initial phases might effectively slow or reverse disease progression.[1] This approach emphasizes identifying early or presymptomatic AD alterations and their targets. In the brains of patients with AD, reduced expression of proliferation markers such as bromodeoxyuridine (BrdU) and nestin, and increased expression of premature neuron markers like doublecortin (DCX) have been observed. However, this does not result in an increase in mature neurons, as decreased neurogenesis is predominantly observed.[2–4] Reduced neurogenesis has been consistently observed in various mouse models for AD.[2,3,5] Furthermore, researchers have found that impaired neurogenesis precedes symptomatic AD.[3] Therefore, understanding how AD-related factors influence neurogenesis is crucial for identifying therapeutic targets and developing strategies to delay or halt the onset and progression of AD.

Despite many efforts to explore biological processes disrupted in the early stages of AD, limited access to the human brain at this stage hampers observing phenotypes of early alterations and validating findings from experimental models. The use of human induced pluripotent stem cells (hiPSCs) has significantly advanced our understanding of AD, especially in clarifying how AD mutations contribute to its pathogenesis. When investigating neurogenesis in AD neural progenitor cells (NPCs), hiPSCs offer a controlled environment for studying the impact of AD mutations. The APP K670N/M671L double mutation (commonly known as the Swedish mutation; APPswe) is a well-established familial AD mutant. Research has shown that, not only in mouse models but also in neurons and cerebral organoids derived from iPSCs of patients carrying this mutation, there is a marked increase in AD-associated phenotypes, such as Aβ accumulation and tau hyperphosphorylation.[6,7] Isogenic cell lines help overcome the genetic variability issues that arise when comparing cells from different donors.

Studies using NPCs and brain organoids generated from hiPSCs derived from patients with AD or engineered to carry AD mutations, have consistently shown impaired neurogenesis, as evidenced by reduced proliferation and premature differentiation.[4,8–12] Here, we aim to investigate the role of AD-related genetic factors in early neurogenesis observed in these hiPSC-derived NPCs and cerebral organoids. By utilizing fluorescence-activated cell sorting (FACS) and RNA sequencing (RNA-seq), we analyzed molecular and cellular

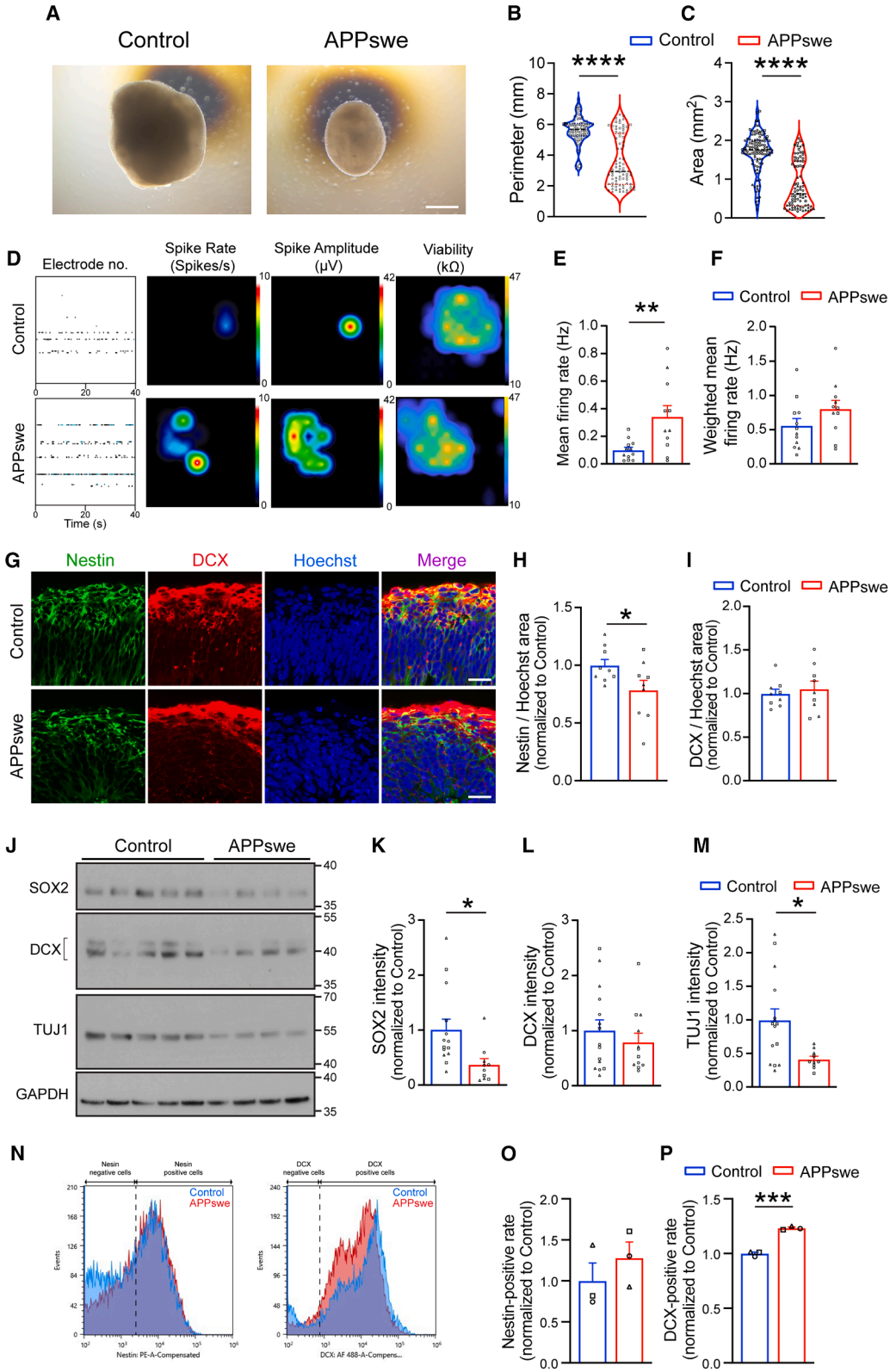

(legend on next page)

changes associated with this phenomenon, which underscored the role of reactive oxygen species (ROS) in early neurogenesis in AD.

RESULTS

Enhanced neuronal activity and early differentiation in APPswe cerebral organoids

We investigated neuronal activity and differentiation in APPswe cerebral organoids at an early stage (cultured for one month) prior to the appearance of extracellular Aβ aggregates.[7] To minimize inter-donor variability, isogenic APPswe hiPSCs were generated from healthy parental cells (female, 75 years old) using CRISPR-Cas9 genome editing and confirmed normal chromosomal architecture and no detectable off-target edits at the top 5 candidate sites (Figures S1A–S1E). This isogenic pair was used to generate cerebral organoids, as established in our previous study.[13] When analyzing organoid size by measuring both perimeter and area, we observed that APPswe cerebral organoids were significantly smaller than the controls (Figures 1A–1C). Multi-electrode array (MEA) recordings exhibited increased frequency and amplitude of neuronal firing in APPswe organoids (Figures 1D and 1E). Viability measurements on the recording plate revealed no difference in recording coverage between the two groups and no difference in the mean firing rate within the active electrodes (Figure 1F). To determine whether these activity differences resulted from variations in the distribution of neuronal populations, we performed immunohistochemistry (IHC) on the surface of cerebral organoids for nestin (NPC marker) and DCX (early neuronal differentiation marker) (Figure 1G). The results revealed a decrease in the nestin-positive area, while the DCX-positive area showed no difference (Figures 1H, 1I, and S1F). This suggests that the increased firing in APPswe organoids is due to a larger neuronal population rather than enhanced firing by individual neurons. To further assess the proportions of NPCs and neurons in cerebral organoids, we conducted immunoblotting for SOX2 (NPC marker), DCX, and TUJ1 (mature neuronal marker) (Figure 1J). The results showed reduced expression of both SOX2 and TUJ1 in APPswe organoids compared to controls (Figures 1K–1M). Additionally, flow cytometry analysis of one-month-old organoids indicated an increased percentage of DCX-positive cells in APPswe organoids compared to controls (Figures 1N–1P). Taken together, these findings suggest that APPswe cerebral organoids exhibit reduced NPC proliferation and accelerated early differentiation that is not accompanied by a corresponding increase in the number of mature neurons.

Increased mitochondrial ROS and its impact on early differentiation in AD NPCs

To further explore the proliferation patterns of NPCs, we performed additional analyses using a 2D culture composed solely of NPCs. APPswe NPCs exhibited decreased nestin and increased DCX expression, which persisted during the one-week neuronal differentiation process (Figures 2A–2C). An EdU incorporation assay revealed reduced proliferation of APPswe NPCs (Figures S2A and S2B). The transition from NPCs to neurons is shown to be associated with increased ROS levels and a shift in glucose metabolism toward oxidative phosphorylation (OXPHOS).[14–18] Staining for mitochondrial ROS using MitoSOX exhibited higher ROS levels in APPswe NPCs (Figures 2D, S2C, and S2D), even though OXPHOS was lower than control NPCs (Figure 2E). This suggests that the elevated ROS in APPswe NPCs was not due to increased OXPHOS. We then investigated whether the increase in mitochondrial ROS levels in APPswe NPCs could be controlled. We found that MitoSOX levels were restored to control levels with EUK8, a mimetic of superoxide dismutase and catalase (Figures S2E and S2F), which ameliorated the early differentiation changes observed in APPswe NPCs (Figures 2F–2H). Next, we examined whether the phenotype observed in APPswe NPCs was present in NPCs containing the APOE4 isoform, which is associated with late-onset AD. Similarly, APOE4 NPCs exhibited decreased nestin expression and increased DCX expression (Figures S2G–S2I), along with higher MitoSOX signal intensity (Figures S5D and S5E). Treatment with EUK8 also mitigated the abnormal differentiation phenotype of APOE4 NPCs (Figures S2J–S2N), suggesting that this phenotype may generally occur under AD conditions.

To determine whether increased ROS levels alone could induce early neuronal differentiation, control NPCs were sorted into high- (top 25%) and low-ROS (bottom 25%) groups, differentiated into neurons, and analyzed for nestin and DCX expression (Figure 2I). No significant differences in nestin or DCX expression were observed between the high- and low-ROS groups (Figures 2J–2L), indicating that elevated ROS alone is insufficient to induce early neuronal differentiation, as observed in AD NPCs.

Transcriptome analysis of APPswe NPCs reveals changes in gene expression toward neuronal differentiation

RNA-seq analysis of APPswe NPCs exhibited upregulation of genes related to neuronal development and synapse signaling, whereas downregulated genes were associated with DNA

Figure 1. Enhanced neuronal activity and early differentiation in APPswe cerebral organoids

(A–C) Quantification of the perimeter (B) and area (C) of control and APPswe cerebral organoids cultured for one month. n = 80–104, from 3 independent differentiations. Scale bar, 500 μm.

(D–F) Neuronal activity was measured by a multi-electrode array in control and APPswe cerebral organoids cultured for one month. n = 11–12, from 3 independent differentiations.

(G–I) Immunohistochemistry was performed to analyze the distribution of (H) nesitn- and (I) DCX-positive cells in control and APPswe cerebral organoids cultured for one month. n = 9, from 3 independent differentiations. Scale bar, 20 μm.

(J–M) Immunoblotting to determine expression levels of SOX2 (K), DCX (L), and TUJ1 (M) in control and APPswe cerebral organoids cultured for one month. n = 10–14, from 3 independent differentiations.

(N–P) Flow cytometry analysis was performed on control and APPswe cerebral organoids cultured for one month to assess the expression levels of (O) nestin- and (P) DCX-positive populations. n = 3 from 3 independent differentiations. $^{*}p < 0.05$, $^{**}p < 0.01$, $^{****}p < 0.0001$ (Student's t test). Error bar ± SEM.

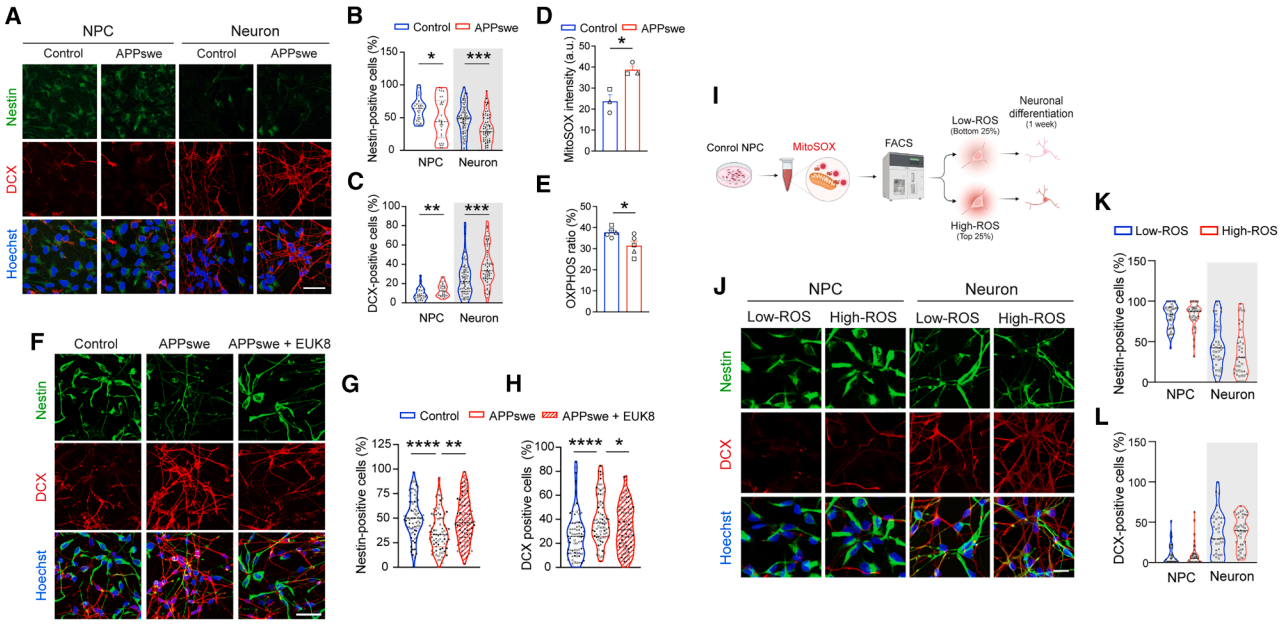

Figure 2. Increased mitochondrial ROS and its impact on early differentiation in APPswe NPCs

(A–C) Immunocytochemistry analysis of nestin (B) and DCX (C) in control and APPswe NPCs and neurons, differentiated for one week. Scale bar, 40 μm. NPCs, $n = 30$, from 3 independent differentiations; neuron, $n = 75$, from 6 independent differentiations.

(D) Increased MitoSOX signal in APPswe NPCs. n = 3, from 3 independent differentiations.

(E) Reduced utilization of OXPHOS in glucose metabolism in APPswe NPCs. n = 5, from 3 independent differentiations.

(F–H) Normalization of increased nestin (G) and decreased DCX (H) expression in APPswe NPCs with EUK8 treatment. Scale bar, 40 μm. n = 75, from 5 independent differentiations.

(I) Schematic of the experiment categorizing control NPCs into high-ROS and low-ROS groups based on MitoSOX signal intensity.

(J–L) No significant differences in nestin and DCX expression between high-ROS and low-ROS NPC groups. Scale bar, 20 μm. n = 40, from 3 independent differentiations. $^{*}p < 0.05$, $^{**}p < 0.01$, $^{***}p < 0.001$, $^{****}p < 0.0001$ (ANOVA test followed by Dunnett's post hoc analysis or Student's t test). Error bar ± SEM.

metabolism and the cell cycle (Figures 3A, S3A, and S3B). SynGO analysis[19] revealed that many of the upregulated genes had synapse-related functions (Figure 3B). However, the expression of genes related to synaptic cleft structure or maintenance did not increase significantly, suggesting that APPswe NPCs may not fully differentiate into mature neurons. We then aimed to determine whether the same transcriptomic changes were observed in control NPCs with elevated ROS expression. We performed gene ontology and SynGO analyses on the intersection of genes with altered transcript expression in APPswe NPCs compared to control NPCs and in high-ROS NPCs compared to low-ROS NPCs. The results revealed that many of the upregulated genes in both APPswe and high-ROS NPCs were related to neuronal development, and commonly downregulated genes were related to DNA metabolism and the cell cycle (Figures S3C–S3F). However, the significance of these changes was reduced compared with the analysis of APPswe NPCs alone. Although the independent analysis of high-ROS NPCs compared to low-ROS NPCs also revealed increased expression of genes related to neuronal development and decreased expression of cell cycle-related genes, these changes were considered insufficient for structural and functional synapse development (Figures S3G–S3J). These results are consistent with the immunocytochemistry findings that showed no difference in nestin and DCX levels between the two groups, suggesting that elevated ROS alone can induce early differentiation but is insufficient to trigger changes toward a neuronal lineage of NPCs.

APPswe NPCs show limited transition to mature neurons and increased vulnerability

To further determine whether APPswe NPCs transitioned into mature neurons, we compared our results with single-cell RNA sequencing (scRNA-seq) data obtained from the human prefrontal cortex at gestation weeks 8–26[20] and examined the changes in cell identity (Figure 3C). Control NPCs closely matched those obtained from the human brain, whereas APPswe NPCs more closely resembled excitatory neurons. Additionally, APPswe NPCs showed increased expression of genes related to oligodendrocyte progenitors, microglia, and astrocytes. High-ROS NPCs exhibited similarities with glia-associated transcriptomic profiles like APPswe NPCs, except they did not show similarities with excitatory neurons. Trajectory analysis confirmed a minimal transition to the neuronal stage in both APPswe and high-ROS NPCs (Figure 3D). Next, we performed weighted gene co-expression network analysis (WGCNA) to identify key regulators of the observed transcriptomic alterations. Given the similarities in the ROS levels and transcriptomic profile patterns between APPswe and high-ROS NPCs, we grouped them together. In addition, we included data from neurons differentiated from high- and low-ROS NPCs in the neuronal category (Figure 3E).

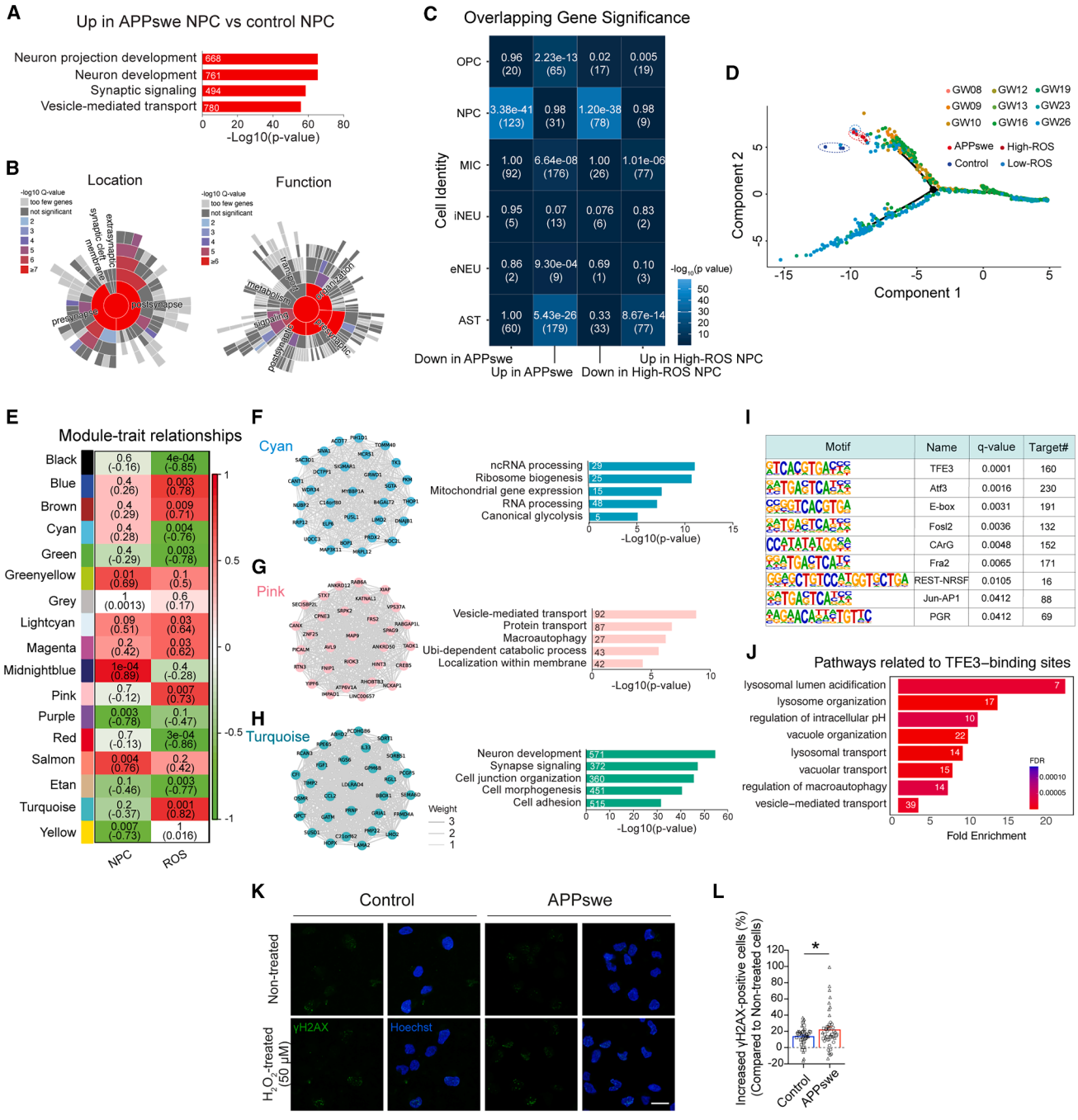

Figure 3. Transcriptional changes indicating early exit from proliferation and increased vulnerability to toxin in APPswe NPCs

(A and B) Gene ontology (GO) analysis (A) and SynGO analysis (B) of genes with increased transcript expression in APPswe NPCs compared to control NPCs, predicting associated biological processes and structural/functional contributions to synapses.

(C) Prediction of cell identity changes by comparing the transcriptomic profiles of APPswe NPCs and high-ROS NPCs with those from developmental stages of the human prefrontal cortex. Color scale represents statistical significance −log10(*p* value). In each box element, the upper value is the *p* value from overlap statistics; the lower value is the overlapping gene count. OPC, oligodendrocyte progenitor cells; MIC, microglial cells; iNEU, inhibitory neurons; eNEU, excitatory neurons; AST, astrocytes.

(D) Trajectory analysis comparing the differentiation status of APPswe NPCs and high-ROS NPCs into neurons with those from developmental stages of the human prefrontal cortex.

(E) Module clustering of genes with expression changes dependent on NPCs and ROS, analyzed through WGCNA. The color scale represents the correlation coefficient. In each box element, the upper value is the *p* value from overlap statistics; the lower value is the correlation coefficient.

(F–H) Key genes (top 30) and gene ontology analysis of modules with significantly altered expression patterns specific to ROS: cyan (F), pink (G), and turquoise (H).

(legend continued on next page)

We identified the cyan, pink, and turquoise modules as gene clusters that were significantly altered by ROS compared to the NPC-specific pattern (Figures 3E–3H). Notably, the turquoise module, which contained the largest number of genes, was associated with neuronal development (Figure 3H). Transcription factor motif analysis suggested that TFE3, a transcription factor upregulated in APPswe and high-ROS NPCs, may regulate the genes within the module (Figures 3I, S3K, and S3L). This regulation could contribute to neuronal differentiation and cellular homeostasis changes by affecting the autophagy-lysosomal pathway (Figure 3J).

Finally, we examined the pathological significance of early differentiation and the transcriptomic alterations observed in APPswe NPCs. These NPC exhibited increased cellular damage markers, such as cleaved-caspase 3 and γ-H2AX (Figures S3M–S3O), and showed heightened susceptibility to damage when exposed to toxins (Figures 3K and 3L). This observation suggests a potential link between early neuronal differentiation, attenuated maturation, and increased vulnerability to toxins in APPswe NPCs, as NPCs are generally more resistant to toxins than their differentiated counterparts.

DISCUSSION

Our study demonstrates that APPswe NPCs exhibit significant transcriptomic changes related to neuron development and synapse signaling while showing reduced expression of genes associated with the DNA metabolic process and cell cycle. However, the incomplete maturation of these cells into fully functional neurons underscores a critical aspect of AD pathology such as impaired neurogenesis in AD. Moreover, the elevated markers of cellular damage and increased susceptibility to toxins highlight the potential pathological consequences of these changes.

Several factors are known to regulate the neuronal differentiation process, with ROS playing a significant role. Although ROS are often considered to have harmful effects, physiological ROS levels are crucial for various cellular functions, including neuronal differentiation.[14] We found that while elevated ROS levels are sufficient to shift the transcriptome profile toward a differentiation state, similar to that in APPswe NPCs, directing the cells toward neuronal differentiation may involve additional intracellular changes driven by AD-causing mutations (e.g., Aβ-induced increase in intracellular Ca^{2+} [21,22]). Several studies have reported a metabolic shift toward oxygen respiration during neurogenesis.[23,24] A recent study using hiPSC showed that increasing energy metabolism by supplementing TCA cycle precursors and essential amino acids facilitated neuronal maturation.[25] In contrast, our research observed a decrease in the OXPHOS ratio in AD NPCs, leading to a more dramatic increase during neuronal differentiation than in control NPCs. This may reflect the early differentiation of AD NPCs and could be a driving force, although it does not serve as an initiation factor.

How do AD-related genetic factors elevate ROS levels? Increased levels of ROS have been well documented in numerous studies from brain samples of AD patients and AD animal models. Various sources could elevate ROS levels in AD brains, such as mitochondrial abnormalities due to reduced expression or impaired function of enzymes for oxidative metabolism, accumulation of Aβ in mitochondrial membranes and intramitochondrial space.[26,27] Significant downregulation of autophagy-related molecules in AD brain samples or AD mouse models suggests impaired autophagy-dependent removal of dysfunctional mitochondria.[28,29] Imbalances of metal ions, such as copper and zinc in AD, can also cause overproduction of ROS.[30,31] However, such ROS increases are more likely to occur in the symptomatic stages of AD. Our study focuses on the role of elevated ROS under physiological conditions rather than pathological ones. We sorted control cells into low ROS (bottom 25%) and high ROS (top 25%) groups and found that one of the significantly enriched GO terms in high-ROS control NPCs was "autophagy." Moreover, we observed normal autophagy activity in AD NPCs despite their increased ROS levels. These findings underscore the importance of physiological ROS levels in regulating autophagy, a concept supported by previous studies such as Scherz-Shouval et al.[32]

scRNA-seq from the brains of AD patients has revealed the heterogeneity of cell types and states within the AD brain, providing unprecedented insights into cellular and molecular complexity. It also allows the uncovering of detailed information about the disease's cellular landscape, including identifying specific cell types and altered pathways over AD progression.[33–35] One key finding from scRNA-seq studies is the altered state of neurogenesis in AD. These studies have shown that AD has an abundance of immature neurons and a disruption in the normal process of neuronal maturation.[2] Our comparative analysis with scRNA-seq data from developing human brains also revealed that APPswe NPCs exhibit transcriptomic profiles similar to those of oligodendrocyte progenitor cells (OPCs) and astrocytes when compared to controls. Since NPCs have the capacity to differentiate into both neurons and glial cells through neurogenesis and gliogenesis, respectively, the upregulation of genes associated with OPCs and astrocytes in APPswe NPCs suggests an increased potential for both pathways. Taken together, these findings indicate that APPswe NPCs have lost their typical progenitor characteristics and are undergoing premature differentiation.

Research from various models for AD, including mouse models, hiPSC-derived neurons, and cerebral organoids, indicates that synaptic weakening is preceded by hyperexcitability.[11,12,36] This observation is also supported by recent scRNA-seq analyses from AD patients,[33–35] suggesting that the dysfunction or reduction of interneurons contributes to an excitation/inhibition imbalance, leading to hyperexcitation in AD brains. Hyperexcitation in glutamatergic neurons consequences neurotoxicity, which can induce neuronal cell death.

(I) Primary transcriptional factors predicted to regulate genes in the turquoise module.
(J) Ontology analysis of genes regulated by TFE3.
(K and L) Increased susceptibility of APPswe NPCs to H_2O_2-induced damage compared to control NPCs. Scale bar, 20μm. n = 45, from 3 independent differentiations. *$p < 0.05$ (Student's t test). Error bar ± SEM.

Our study observed that AD NPCs-derived neurons exhibited heightened sensitivity to extracellular toxins. This sensitivity could elucidate the reduced neurogenesis observed in the hyperexcitation environments of AD brains. The increased neuronal activity in AD brains not only leads to neurotoxicity but may also contribute to the overproduction of Aβ,[37–39] which in turn promotes premature differentiation of NPCs. Our findings linking hyperexcitation, premature differentiation, and increased vulnerability of AD NPCs provide a new perspective on the underlying mechanisms of AD and open new avenues for therapeutic interventions targeting these pathways. For example, by normalizing the abnormally elevated ROS levels in AD NPCs, it may be possible to suppress early neuronal differentiation and promote the formation of mature neurons.

Limitations of the study

In this study, we propose that premature differentiation of NPCs induced by the APPswe mutation may contribute to reduced neurogenesis observed in AD brains. However, further studies are required to directly determine whether this phenomenon in the adult AD brain is mediated by increased ROS, as demonstrated in our findings, and whether it can be normalized through ROS inhibition. Additionally, direct investigation is necessary to confirm whether transcription factors such as TFE3, suggested by our study, indeed function as key regulators in this pathological process. Finally, it will also be important to determine whether similar phenomena generally occur in other AD cases, such as those associated with APOE4 as observed in our study. Such findings would be critical for developing novel therapeutic strategies targeting early-stage AD pathology.

RESOURCE AVAILABILITY

Lead contact

Further requests for the resources and reagents should be directed to and will be fulfilled by the lead contact, Jinsoo Seo (jseo@yonsei.ac.kr).

Materials availability

All unique materials and reagents will be available from the lead contact with a completed materials transfer agreement upon request.

Data and code availability

- RNA-seq data that support the findings of this study are deposited in the Gene Expression Omnibus. https://www.ncbi.nlm.nih.gov/geo/query/acc.cgi?acc=GSE274912. Original western blot images have been deposited at Mendeley and are publicly available as of the date of publication. The DOI is listed in the key resources table.
- This paper does not report the original code.
- Any additional information required to reanalyze the data reported in this paper is available from the lead contact upon request.

ACKNOWLEDGMENTS

The authors would like to thank all members of the Seo lab for their advice and discussion. This work was supported by the UK Dementia Research Institute (award number: UKDRI-5016) through UK DRI Ltd, principally funded by the Medical Research Council and by the Lily Safra and the Edmond J. Safra Foundation to A.N. and the National Research Foundation (NRF) grants funded by the Ministry of Science and ICT (MSIT), South Korea (grant number: 2022R1A2C4001611, RS-2023-00266171) and the POSCO Science Fellowship of POSCO TJ Park Foundation to J.S. All schematics were created using BioRender with a full license to publish.

AUTHOR CONTRIBUTIONS

J.C. and J.S. designed the project and wrote the manuscript. J.C., S.B., J.J., and C.L. performed experiments. J.C., S.B., J.J., J.T., C.L., A.N., F.G., and J.S. analyzed the data.

DECLARATION OF INTERESTS

The authors declare no competing interests.

STAR★METHODS

Detailed methods are provided in the online version of this paper and include the following:

- KEY RESOURCES TABLE
- EXPERIMENTAL MODEL AND STUDY PARTICIPANT DETAILS
  - Human-induced pluripotent stem cells (hiPSCs)
- METHOD DETAILS
  - Generation of isogenic iPSC lines
  - hiPSCs culture
  - Neural Progenitor Cell (NPC) differentiation from hiPSCs
  - Neuron differentiation from NPCs
  - Cerebral organoid Generation from hiPSCs
  - Multi-electrode Array (MEA) recording and analysis
  - Immunohistochemistry
  - Immunoblotting
  - Flow cytometry analysis from cerebral organoids
  - Immunocytochemistry
  - Seahorse extracellular analysis
  - EdU staining
  - MitoSOX staining and Fluorescence-activated Cell Sorting (FACS)
  - Transcriptomic analysis
  - Transcription factor binding motif enrichment
- QUANTIFICATION AND STATISTICAL ANALYSIS

SUPPLEMENTAL INFORMATION

Supplemental information can be found online at https://doi.org/10.1016/j.isci.2025.112446.

Received: November 11, 2024
Revised: February 26, 2025
Accepted: April 11, 2025
Published: April 16, 2025

REFERENCES

1. Boxer, A.L., and Sperling, R. (2023). Accelerating Alzheimer's therapeutic development: The past and future of clinical trials. Cell *186*, 4757–4772. https://doi.org/10.1016/j.cell.2023.09.023.
2. Salta, E., Lazarov, O., Fitzsimons, C.P., Tanzi, R., Lucassen, P.J., and Choi, S.H. (2023). Adult hippocampal neurogenesis in Alzheimer's disease: A roadmap to clinical relevance. Cell Stem Cell *30*, 120–136. https://doi.org/10.1016/j.stem.2023.01.002.
3. Mu, Y., and Gage, F.H. (2011). Adult hippocampal neurogenesis and its role in Alzheimer's disease. Mol. Neurodegener. *6*, 85. https://doi.org/10.1186/1750-1326-6-85.
4. Arber, C., Lovejoy, C., Harris, L., Willumsen, N., Alatza, A., Casey, J.M., Lines, G., Kerins, C., Mueller, A.K., Zetterberg, H., et al. (2021). Familial Alzheimer's Disease Mutations in PSEN1 Lead to Premature Human Stem Cell Neurogenesis. Cell Rep. *34*, 108615. https://doi.org/10.1016/j.celrep.2020.108615.

5. Scopa, C., Marrocco, F., Latina, V., Ruggeri, F., Corvaglia, V., La Regina, F., Ammassari-Teule, M., Middei, S., Amadoro, G., Meli, G., et al. (2020). Impaired adult neurogenesis is an early event in Alzheimer's disease neurodegeneration, mediated by intracellular Aβ oligomers. Cell Death Differ. *27*, 934–948. https://doi.org/10.1038/s41418-019-0409-3.

6. Israel, M.A., Yuan, S.H., Bardy, C., Reyna, S.M., Mu, Y., Herrera, C., Hefferan, M.P., Van Gorp, S., Nazor, K.L., Boscolo, F.S., et al. (2012). Probing sporadic and familial Alzheimer's disease using induced pluripotent stem cells. Nature *482*, 216–220. https://doi.org/10.1038/nature10821.

7. Raja, W.K., Mungenast, A.E., Lin, Y.-T., Ko, T., Abdurrob, F., Seo, J., and Tsai, L.-H. (2016). Self-Organizing 3D Human Neural Tissue Derived from Induced Pluripotent Stem Cells Recapitulate Alzheimer's Disease Phenotypes. PLoS One *11*, e0161969. https://doi.org/10.1371/journal.pone.0161969.

8. Yang, J., Zhao, H., Ma, Y., Shi, G., Song, J., Tang, Y., Li, S., Li, T., Liu, N., Tang, F., et al. (2017). Early pathogenic event of Alzheimer's disease documented in iPSCs from patients with PSEN1 mutations. Oncotarget *8*, 7900–7913. https://doi.org/10.18632/oncotarget.13776.

9. Zhao, J., Fu, Y., Yamazaki, Y., Ren, Y., Davis, M.D., Liu, C.-C., Lu, W., Wang, X., Chen, K., Cherukuri, Y., et al. (2020). APOE4 exacerbates synapse loss and neurodegeneration in Alzheimer's disease patient iPSC-derived cerebral organoids. Nat. Commun. *11*, 5540. https://doi.org/10.1038/s41467-020-19264-0.

10. Vanova, T., Sedmik, J., Raska, J., Amruz Cerna, K., Taus, P., Pospisilova, V., Nezvedova, M., Fedorova, V., Kadakova, S., Klimova, H., et al. (2023). Cerebral organoids derived from patients with Alzheimer's disease with PSEN1/2 mutations have defective tissue patterning and altered development. Cell Rep. *42*, 113310. https://doi.org/10.1016/j.celrep.2023.113310.

11. Meyer, K., Feldman, H.M., Lu, T., Drake, D., Lim, E.T., Ling, K.-H., Bishop, N.A., Pan, Y., Seo, J., Lin, Y.-T., et al. (2019). REST and Neural Gene Network Dysregulation in iPSC Models of Alzheimer's Disease. Cell Rep. *26*, 1112–1127.e9. https://doi.org/10.1016/j.celrep.2019.01.023.

12. Lin, Y.-T., Seo, J., Gao, F., Feldman, H.M., Wen, H.-L., Penney, J., Cam, H. P., Gjoneska, E., Raja, W.K., Cheng, J., et al. (2018). APOE4 Causes Widespread Molecular and Cellular Alterations Associated with Alzheimer's Disease Phenotypes in Human iPSC-Derived Brain Cell Types. Neuron *98*, 1141–1154.e7. https://doi.org/10.1016/j.neuron.2018.05.008.

13. Park, J.-H., Hwang, J.-W., Lee, H.J., Jang, G.M., Jeong, Y.J., Cho, J., Seo, J., and Hoe, H.-S. (2023). Lomerizine inhibits LPS-mediated neuroinflammation and tau hyperphosphorylation by modulating NLRP3, DYRK1A, and GSK3α/β. Front. Immunol. *14*, 1150940. https://doi.org/10.3389/fimmu.2023.1150940.

14. Sies, H., and Jones, D.P. (2020). Reactive oxygen species (ROS) as pleiotropic physiological signalling agents. Nat. Rev. Mol. Cell Biol. *21*, 363–383. https://doi.org/10.1038/s41580-020-0230-3.

15. Jang, Y.-Y., and Sharkis, S.J. (2007). A low level of reactive oxygen species selects for primitive hematopoietic stem cells that may reside in the low-oxygenic niche. Blood *110*, 3056–3063. https://doi.org/10.1182/blood-2007-05-087759.

16. Konopka, R., Kubala, L., Lojek, A., and Pacherník, J. (2008). Alternation of retinoic acid induced neural differentiation of P19 embryonal carcinoma cells by reduction of reactive oxygen species intracellular production. Neuroendocrinol. Lett. *29*, 770–774.

17. Tsatmali, M., Walcott, E.C., Makarenkova, H., and Crossin, K.L. (2006). Reactive oxygen species modulate the differentiation of neurons in clonal cortical cultures. Mol. Cell. Neurosci. *33*, 345–357. https://doi.org/10.1016/j.mcn.2006.08.005.

18. Suzukawa, K., Miura, K., Mitsushita, J., Resau, J., Hirose, K., Crystal, R., and Kamata, T. (2000). Nerve Growth Factor-induced Neuronal Differentiation Requires Generation of Rac1-regulated Reactive Oxygen Species. J. Biol. Chem. *275*, 13175–13178. https://doi.org/10.1074/jbc.275.18.13175.

19. Koopmans, F., van Nierop, P., Andres-Alonso, M., Byrnes, A., Cijsouw, T., Coba, M.P., Cornelisse, L.N., Farrell, R.J., Goldschmidt, H.L., Howrigan, D.P., et al. (2019). SynGO: An Evidence-Based, Expert-Curated Knowledge Base for the Synapse. Neuron *103*, 217–234.e4. https://doi.org/10.1016/j.neuron.2019.05.002.

20. Zhong, S., Zhang, S., Fan, X., Wu, Q., Yan, L., Dong, J., Zhang, H., Li, L., Sun, L., Pan, N., et al. (2018). A single-cell RNA-seq survey of the developmental landscape of the human prefrontal cortex. Nature *555*, 524–528. https://doi.org/10.1038/nature25980.

21. Kuchibhotla, K.V., Goldman, S.T., Lattarulo, C.R., Wu, H.-Y., Hyman, B.T., and Bacskai, B.J. (2008). Aβ Plaques Lead to Aberrant Regulation of Calcium Homeostasis In Vivo Resulting in Structural and Functional Disruption of Neuronal Networks. Neuron *59*, 214–225. https://doi.org/10.1016/j.neuron.2008.06.008.

22. Calvo-Rodriguez, M., Hou, S.S., Snyder, A.C., Kharitonova, E.K., Russ, A. N., Das, S., Fan, Z., Muzikansky, A., Garcia-Alloza, M., Serrano-Pozo, A., et al. (2020). Increased mitochondrial calcium levels associated with neuronal death in a mouse model of Alzheimer's disease. Nat. Commun. *11*, 2146. https://doi.org/10.1038/s41467-020-16074-2.

23. Zheng, X., Boyer, L., Jin, M., Mertens, J., Kim, Y., Ma, L., Ma, L., Hamm, M., Gage, F.H., and Hunter, T. (2016). Metabolic reprogramming during neuronal differentiation from aerobic glycolysis to neuronal oxidative phosphorylation. Elife *5*, e13374. https://doi.org/10.7554/elife.13374.

24. Arrázola, M.S., Andraini, T., Szelechowski, M., Mouledous, L., Arnauné-Pelloquin, L., Davezac, N., Belenguer, P., Rampon, C., and Miquel, M.-C. (2019). Mitochondria in Developmental and Adult Neurogenesis. Neurotox. Res. *36*, 257–267. https://doi.org/10.1007/s12640-018-9942-y.

25. Bifari, F., Dolci, S., Bottani, E., Pino, A., Di Chio, M., Zorzin, S., Ragni, M., Zamfir, R.G., Brunetti, D., Bardelli, D., et al. (2020). Complete neural stem cell (NSC) neuronal differentiation requires a branched chain amino acids-induced persistent metabolic shift towards energy metabolism. Pharmacol. Res. *158*, 104863. https://doi.org/10.1016/j.phrs.2020.104863.

26. Mary, A., Eysert, F., Checler, F., and Chami, M. (2023). Mitophagy in Alzheimer's disease: Molecular defects and therapeutic approaches. Mol. psychiatry *28*, 202–216. https://doi.org/10.1038/s41380-022-01631-6.

27. Tönnies, E., and Trushina, E. (2017). Oxidative Stress, Synaptic Dysfunction, and Alzheimer's Disease. J. Alzheimer's Dis. *57*, 1105–1121. https://doi.org/10.3233/jad-161088.

28. Pomilio, C., Gorojod, R.M., Riudavets, M., Vinuesa, A., Presa, J., Gregosa, A., Bentivegna, M., Alaimo, A., Alcon, S.P., Sevlever, G., et al. (2020). Microglial autophagy is impaired by prolonged exposure to β-amyloid peptides: evidence from experimental models and Alzheimer's disease patients. GeroScience *42*, 613–632. https://doi.org/10.1007/s11357-020-00161-9.

29. Lachance, V., Wang, Q., Sweet, E., Choi, I., Cai, C.-Z., Zhuang, X.-X., Zhang, Y., Jiang, J.L., Blitzer, R.D., Bozdagi-Gunal, O., et al. (2019). Autophagy protein NRBF2 has reduced expression in Alzheimer's brains and modulates memory and amyloid-beta homeostasis in mice. Mol. Neurodegener. *14*, 43. https://doi.org/10.1186/s13024-019-0342-4.

30. Cheignon, C., Tomas, M., Bonnefont-Rousselot, D., Faller, P., Hureau, C., and Collin, F. (2018). Oxidative stress and the amyloid beta peptide in Alzheimer's disease. Redox Biol. *14*, 450–464. https://doi.org/10.1016/j.redox.2017.10.014.

31. Wang, L., Yin, Y.-L., Liu, X.-Z., Shen, P., Zheng, Y.-G., Lan, X.-R., Lu, C.-B., and Wang, J.-Z. (2020). Current understanding of metal ions in the pathogenesis of Alzheimer's disease. Transl. Neurodegener. *9*, 10. https://doi.org/10.1186/s40035-020-00189-z.

32. Scherz-Shouval, R., Shvets, E., and Elazar, Z. (2007). Oxidation as a Post-Translational Modification that Regulates Autophagy. Autophagy *3*, 371–373. https://doi.org/10.4161/auto.4214.

33. Gazestani, V., Kamath, T., Nadaf, N.M., Dougalis, A., Burris, S.J., Rooney, B., Junkkari, A., Vanderburg, C., Pelkonen, A., Gomez-Budia, M., et al. (2023). Early Alzheimer's disease pathology in human cortex involves

transient cell states. Cell *186*, 4438–4453.e23. https://doi.org/10.1016/j.cell.2023.08.005.

34. Luo, W., Qu, W., and Gan, L. (2023). The AD odyssey 2023: Tales of single cell. Cell *186*, 4257–4259. https://doi.org/10.1016/j.cell.2023.09.001.
35. Mathys, H., Peng, Z., Boix, C.A., Victor, M.B., Leary, N., Babu, S., Abdelhady, G., Jiang, X., Ng, A.P., Ghafari, K., et al. (2023). Single-cell atlas reveals correlates of high cognitive function, dementia, and resilience to Alzheimer's disease pathology. Cell *186*, 4365–4385.e27. https://doi.org/10.1016/j.cell.2023.08.039.
36. Ghatak, S., Dolatabadi, N., Trudler, D., Zhang, X., Wu, Y., Mohata, M., Ambasudhan, R., Talantova, M., and Lipton, S.A. (2019). Mechanisms of hyperexcitability in Alzheimer's disease hiPSC-derived neurons and cerebral organoids vs isogenic controls. Elife *8*, e50333. https://doi.org/10.7554/elife.50333.
37. Bero, A.W., Yan, P., Roh, J.H., Cirrito, J.R., Stewart, F.R., Raichle, M.E., Lee, J.-M., and Holtzman, D.M. (2011). Neuronal activity regulates the regional vulnerability to amyloid-β deposition. Nat. Neurosci. *14*, 750–756. https://doi.org/10.1038/nn.2801.
38. Das, U., Scott, D.A., Ganguly, A., Koo, E.H., Tang, Y., and Roy, S. (2013). Activity-Induced Convergence of APP and BACE-1 in Acidic Microdomains via an Endocytosis-Dependent Pathway. Neuron *79*, 447–460. https://doi.org/10.1016/j.neuron.2013.05.035.
39. Cirrito, J.R., Kang, J.-E., Lee, J., Stewart, F.R., Verges, D.K., Silverio, L.M., Bu, G., Mennerick, S., and Holtzman, D.M. (2008). Endocytosis Is Required for Synaptic Activity-Dependent Release of Amyloid-β In Vivo. Neuron *58*, 42–51. https://doi.org/10.1016/j.neuron.2008.02.003.
40. Dobin, A., Davis, C.A., Schlesinger, F., Drenkow, J., Zaleski, C., Jha, S., Batut, P., Chaisson, M., and Gingeras, T.R. (2013). STAR: ultrafast universal RNA-seq aligner. Bioinformatics *29*, 15–21. https://doi.org/10.1093/bioinformatics/bts635.
41. Liao, Y., Smyth, G.K., and Shi, W. (2014). featureCounts: an efficient general purpose program for assigning sequence reads to genomic features. Bioinformatics *30*, 923–930. https://doi.org/10.1093/bioinformatics/btt656.
42. Love, M.I., Huber, W., and Anders, S. (2014). Moderated estimation of fold change and dispersion for RNA-seq data with DESeq2. Genome Biol. *15*, 550. https://doi.org/10.1186/s13059-014-0550-8.
43. Chen, J., Bardes, E.E., Aronow, B.J., and Jegga, A.G. (2009). ToppGene Suite for gene list enrichment analysis and candidate gene prioritization. Nucleic Acids Res. *37*, W305–W311. https://doi.org/10.1093/nar/gkp427.
44. Heinz, S., Benner, C., Spann, N., Bertolino, E., Lin, Y.C., Laslo, P., Cheng, J.X., Murre, C., Singh, H., and Glass, C.K. (2010). Simple Combinations of Lineage-Determining Transcription Factors Prime cis-Regulatory Elements Required for Macrophage and B Cell Identities. Mol. Cell *38*, 576–589. https://doi.org/10.1016/j.molcel.2010.05.004.
45. Mi, H., Muruganujan, A., Huang, X., Ebert, D., Mills, C., Guo, X., and Thomas, P.D. (2019). Protocol Update for large-scale genome and gene function analysis with the PANTHER classification system (v.14.0). Nat. Protoc. *14*, 703–721. https://doi.org/10.1038/s41596-019-0128-8.
46. Qiu, X., Mao, Q., Tang, Y., Wang, L., Chawla, R., Pliner, H.A., and Trapnell, C. (2017). Reversed graph embedding resolves complex single-cell trajectories. Nat. Methods *14*, 979–982. https://doi.org/10.1038/nmeth.4402.
47. Langfelder, P., and Horvath, S. (2008). WGCNA: an R package for weighted correlation network analysis. BMC Bioinform. *9*, 559. https://doi.org/10.1186/1471-2105-9-559.
48. Gupta, S., Stamatoyannopoulos, J.A., Bailey, T.L., and Noble, W.S. (2007). Quantifying similarity between motifs. Genome Biol. *8*, R24. https://doi.org/10.1186/gb-2007-8-2-r24.

STAR★METHODS

KEY RESOURCES TABLE

REAGENT or RESOURCE	SOURCE	IDENTIFIER
Antibodies		
Anti-SOX2 antibody	Abcam	Cat# ab97959; RRID:AB_2341193
Anti-Doublecortin (DCX) antibody	Abcam	Cat# ab18723; RRID:AB_732011
Neuronal Class III beta-Tubulin (TUJ1) Monoclonal Antibody, Purified	BioLegend	Cat# 801201; RRID:AB_2313773
GAPDH (6C5)	Santa Cruz Biotechnology	Cat# sc-32233; RRID:AB_627679
Anti-Nestin, human, clone 10C2	Millipore	Cat# MAB5326; RRID:AB_2251134
Human Nestin Phycoerythrin (PE)-conjugated Antibody	R&D Systems	Cat# IC1259P; RRID:AB_2151147
Cleaved Caspase-3 (Asp175) (5A1E) Rabbit mAb	Cell Signaling Technology	Cat# 9664; RRID:AB_2070042
Anti-phospho-Histone H2A.X (Ser139) Antibody, clone JBW301	Millipore	Cat# 05-636; RRID:AB_309864
Chemicals, peptides, and recombinant proteins		
hESC-qualified matrigel	Corning	Cat# 356277
mTeSR1	StemCell Technologies	Cat# 85850
DMEM/F-12, GlutaMAX™ supplement	Gibco	Cat# 10565018
Neurobasal™ Medium	Gibco	Cat# 21103049
MEM Non-essential Amino Acid Solution (100×)	Merck	Cat# M7145
GlutaMAX™ Supplement	Gibco	Cat# 35050061
Insulin solution human	Sigma-Aldrich	Cat# I9278
2-Mercaptoethanol	Sigma-Aldrich	Cat# M3148
Penicillin-Streptomycin (10,000 U/mL)	Gibco	Cat# 15140122
B-27™ supplement (50X), serum free	Gibco	Cat# 17504044
N-2 Supplement (100X)	Gibco	Cat# 17502001
Dorsomorphin dihydrochloride	Tocris	Cat# 3093
SB 431542	Tocris	Cat# 1614
Recombinant Human FGF-basic (154 a.a.)	PeproTech	Cat# 100-18B
ACCUTASE™	StemCell Technologies	Cat# 07922
Recombinant Human/Murine/Rat BDNF	PeproTech	Cat# 450-02
Recombinant Human GDNF	PeproTech	Cat# 450-10
Glasgow's MEM (GMEM)	Gibco	Cat# 11710035
KnockOut™ Serum Replacement	Gibco	Cat# 10828010
Sodium Pyruvate (100 mM)	Gibco	Cat# 11360070
endo-IWR 1	Tocris	Cat# 3532
Chemically Defined Lipid Concentrate	Gibco	Cat# 11905031
DPBS	Biowest	Cat# L0615-500
Tris	Duchefa Biochemie	Cat# T1501
NaCl	Sigma-Aldrich	Cat# 9888
NP-40	Sigma-Aldrich	Cat# I8896
Sodium deoxycholate	Sigma-Aldrich	Cat# 264103
SDS	Sigma-Aldrich	Cat# 62862
Triton™ X-100	Sigma-Aldrich	Cat# T9284
BSA assay kit	Bio-Rad	Cat# 5000006
Tween® 20, Molecular Biology Grade	Promega	Cat# H5151
Fisher Healthcare Tissue-Plus™ O.C.T. Compound	Thermo Fisher Scientific	Cat# 23-730-571
Skim Milk Powder	MB cell	Cat# MB-S1667

(*Continued on next page*)

Continued

REAGENT or RESOURCE	SOURCE	IDENTIFIER
Albumin bovine, fraction V, ≥98%	MP Biomedicals	Cat# 0216006980
Donkey serum	Merck	Cat# S30-100ML
Glycine	Daejung	Cat# 4068-4105
Hoechst 33342	Invitrogen	Cat# H3570
MitoSOX	Invitrogen	Cat# M36008
Live-or-Dye™ Fixable Viability Staining Kits	Biotium	Cat# 32008-T
XF 24 FLUXPAK MINI	Agilent Technologies	Cat# 102342-100
XF DMEM medium	Agilent Technologies	Cat# 103573-100
Seahorse XF Glucose Solution	Agilent Technologies	Cat# 103577-100
Seahorse XF Pyruvate Solution	Agilent Technologies	Cat# 103578-100
Seahorse XF Glutamine Solution	Agilent Technologies	Cat# 103579-100
Oligomycin	Sigma-Aldrich	Cat# 75351
2-Deoxy-D-glucose	Sigma-Aldrich	Cat# 8375
FCCP [carbonyl cyanide 4-(trifluoromethoxy)-phenylhydrazone]	Sigma-Aldrich	Cat# C2920
Rotenone	Sigma-Aldrich	Cat# R8875
Critical commercial assays		
Click-iT™ EdU Cell Proliferation Kit for Imaging, Alexa Fluor™ 594 dye EdU	Invitrogen	Cat# C10339
P3 Primary Cell 4D-Nucleofector Kit	Lonza	Cat# V4XP-3024
Deposited data		
scRNA-seq from human prefrontal cortex at gestation weeks 8-26	Zhong et al.[20]	GEO: GSE274912
RNA-seq data from NPCs and Neurons	In this study	GEO: GSE104276
Original western blot images	In this study	https://doi.org/10.17632/zjcy22ztjr.1 (Mendeley Data)
Experimental models: Cell lines		
Human iPSC line from a healthy control (*APOE3*)	Coriell	Cat# AG09173
APOE4 isogenic line from #AG09173	Tsai Laboratory[12]	N/A
APPswe isogenic line from #AG09713	In this study	N/A
Oligonucleotides		
APP sgRNA oligomer pair (Forward): 5'–CACCGCAGAATTCCGACATGACTC-3'	This paper	N/A
APP sgRNA oligomer pair (Reverse): 5'–AAACGAGTCATGTCGGAATTCTGC-3'	This paper	N/A
ssODN for APP → APPswe 5'-AAACTAATTGGTTGTCCTGCATACT TTAATTATGATGTAATACAGGTTCTGG GTTGACAAATATCAAGACGGAGGAGA TCTCTGAAGTGAATCTCGATGCAGAAT TCCGACATGACTCAGGATATGAAGTT CATCATCAAAAATTGGTACGTAAAAT AATTTACCTCTTTCCACTACTGT-3'	This paper	N/A
Primer for APP (Forward): 5'-GCCAACCTCTCAACCAGGAT-3'	This paper	N/A
Primer for APP (Reverse): 5'-GCACAGGATGAACCAGAGTT-3'	This paper	N/A
Primer for Off-target #1 (Forward): 5'-GATGACTAAGTAGAGTTGGGGAGC-3'	This paper	N/A
Primer for Off-target #1 (Reverse): 5'-GACAATAGCGGTTTTGATGG-3'	This paper	N/A

(*Continued on next page*)

Continued

REAGENT or RESOURCE	SOURCE	IDENTIFIER
Primer for Off-target #2 (Forward): 5'-AGGAACAGCCTGCACATAGC-3'	This paper	N/A
Primer for Off-target #2 (Reverse): 5'-GGTGTGGATCTCAGTGGCTC-3'	This paper	N/A
Primer for Off-target #3 (Forward): 5'-AAGCACCAGTAGCCTTGACC-3'	This paper	N/A
Primer for Off-target #3 (Reverse): 5'-TGGCCAGAAGGACATAAGCC-3'	This paper	N/A
Primer for Off-target #4 (Forward): 5'-CCTGACTGGGGGATTAGGGA-3'	This paper	N/A
Primer for Off-target #4 (Reverse): 5'-GGTGCCATTCTTGGCTCTCT-3'	This paper	N/A
Primer for Off-target #5 (Forward): 5'-GGTTCCTGCTCCATCGTTCC-3'	This paper	N/A
Primer for Off-target #5 (Reverse): 5'-CGTTCATCCGTTACTGTCCAC-3'	This paper	N/A
Recombinant DNA		
pSpCas9(BB)-2A-GFP (PX458)	Addgene	Cat#43138, RRID:Addgene_48138
Software and algorithms		
AxIS	https://www.axionbiosystems.com/products/axis-software	RRID:SCR_016308
Neural Module	https://www.axionbiosystems.com/products/software/neural-module	RRID:SCR_019270
Sony Biotechnology SH800S Cell Sorter	https://www.sonybiotechnology.com/us/instruments/sh800s-cell-sorter/	RRID:SCR_018066
GraphPad Prism	http://www.graphpad.com/	RRID:SCR_002798
Seahorse Wave	Agilent Technologies	RRID:SCR_014526
STAR (v.2.4.0)	Dobin et al.[40]	N/A
featureCounts	Liao et al.[41]	N/A
DESeq2 (v1.26.0)	Love et al.[42]	N/A
ToppGene Suite	Chen et al.[43]	N/A
SynGO	Koopmans et al.[19]	N/A
HOMER	Heinz et al.[44]	N/A
PANTHER	Mi et al.[45]	N/A

EXPERIMENTAL MODEL AND STUDY PARTICIPANT DETAILS

Human-induced pluripotent stem cells (hiPSCs)

Unaffected hiPSCs carrying the APOE3 genotype were obtained from a 75-year-old female donor (Coriell #AG09173). The Institutional Review Board (IRB) of Daegu Gyeongbuk Institute for Science and Technology approved the use of human iPSCs (Permit Number: DGIST-190829-BR-071-01). Isogenic APPswe hiPSC lines were generated from this unaffected line using CRISPR/Cas9 technology with a single guide RNA (sgRNA; key resources table) and a single-stranded oligodeoxynucleotide (ssODN; key resources table) as described in the 'method details' section. The top 5 off-target sites were predicted using http://tools.genome-engineering.org, and the primer sets for sequencing are provided in the key resources table. Additionally, we utilized the ApoE4 isogenic iPSC line generated previously from the same control line.[12]

METHOD DETAILS

Generation of isogenic iPSC lines

The sgRNAs designed to target the APP gene near the site of the APPswe mutation introduction (key resources table) were annealed and cloned into the pSpCas9-2A-GFP (PX458) vector (Addgene #48138). The resulting plasmid was introduced into human induced pluripotent stem cells (hiPSCs) by electroporation using a Amaxa 4D-Nucleofector system and the P3 Primary Cell 4D Nucleofector Kit (Lonza). Briefly, 1×10^6 hiPSCs were resuspended in 100 μL of the provided reaction buffer, followed by the addition of 3 μg of

plasmid DNA and 6 μg of single-stranded oligodeoxynucleotide (ssODN; key resources table) carrying the APPswe mutation sequence. Two days post-electroporation, GFP-positive hiPSCs were isolated by fluorescence-activated cell sorting (FACS; Sony SH800S).

hiPSCs culture

The iPSCs were cultured on hESC-qualified Matrigel (Corning)-coated culture plates and maintained in mTeSR1 media (StemCell Technologies). The culture media was replaced daily to ensure optimal growth and maintenance of the iPSCs.

Neural Progenitor Cell (NPC) differentiation from hiPSCs

For the differentiation of NPCs from hiPSCs, the iPSCs were initially cultured on 6-well plates coated with hESC-qualified Matrigel in mTeSR1 media until they reached approximately 100% confluence, forming a single layer. The media was then replaced with neural induction media, which comprised DMEM/F-12 GlutaMAX (Gibco), Neurobasal (Gibco), 0.5x NEAA (Merck), 0.5x GlutaMAX (Gibco), 5 μg/ml insulin (Sigma-Aldrich), 100 μM 2-mercaptoethanol (Sigma-Aldrich), 1x Penicillin/Streptomycin (Gibco), 0.5x B-27 (Gibco), and 0.5x N-2 (Gibco). This media also contained 1 μM Dorsomorphin (Tocris) and 10 μM SB431542 (Tocris) and was used for 11 days. After this induction period, the cells were dissociated using Accutase (StemCell Technologies) and passaged onto a new 6-well plate coated with Matrigel. The cells continued to be cultured in the neural induction media until the appearance of neural rosette structures. Once the neural rosettes formed, the cells were passaged again to a new 6-well plate at a density of 4 x 10^6 cells per well and maintained in neural induction media supplemented with 20 ng/ml FGF2 (Peprotech). The media was changed every other day to support the maintenance and proliferation of NPCs.

Neuron differentiation from NPCs

For neuronal differentiation, NPCs were dissociated using Accutase (StemCell Technologies) and then plated onto a cell culture plate coated with Matrigel. The following day, the media was replaced with neural differentiation media, which consisted of the neural induction media supplemented with 10 ng/ml BDNF (Peprotech) and 10 ng/ml GDNF (Peprotech). The cells were maintained in this neural differentiation media for one week, with half of the media being changed every three days to ensure the optimal environment for neuronal differentiation.

Cerebral organoid Generation from hiPSCs

hiPSCs on Matrigel-coated plates were first dissociated using Accutase (StemCell Technologies). The cells were then seeded at a density of 12,000 cells per well into U-shaped 96-well plates (Corning). The cells were maintained in embryoid body (EB) formation media, which consisted of Glasgow's MEM (Gibco), 20% knockout serum replacement (Gibco), 1x sodium pyruvate (Gibco), 1x NEAA, 0.1 mM 2-mercaptoethanol, 3 μM endo-IWR-1 (Tocris), and 5 μM SB431542, along with 20 μM Rock inhibitor, for 18–20 days. Additionally, 2 μM Dorsomorphin was added to the EB formation media for the first three days. The media was changed every other day. On days 18–20, the EBs were transferred, one per well, to a 24-well plate. The media was then replaced with neural induction media, consisting of DMEM/F-12 GlutaMAX, 1x N-2, and 1x Chemically Defined Lipid Concentrate (Gibco). The cells were maintained in an incubator with a 40% oxygen condition. The cerebral organoids were used for experiments at one month of differentiation. To measure the size of cerebral organoids, the organoids were imaged using an MC170 HD camera (Leica). The obtained images were analyzed using ImageJ software (NIH). We outlined the organoids and measured their total perimeter and area to assess their size.

Multi-electrode Array (MEA) recording and analysis

For MEA recordings, one-month-old cerebral organoids were plated on 6-well CytoView MEA plates (Axion BioSystems) that had been coated with a 0.1% PEI solution. Recordings were conducted using the Maestro Edge MEA platform (Axion BioSystems, USA) maintained at 37°C and 5% CO2. Real-time data collection was performed simultaneously across all 64 electrodes. The data was analyzed using AxIS Navigator and AxIS Neural Metrics tool software (Axion BioSystems).

Immunohistochemistry

One-month-old cerebral organoids were first washed three times with DPBS and then fixed overnight at 4°C in a 4% paraformaldehyde (PFA) solution. After fixation, the organoids were washed again three times with DPBS before being incubated overnight at 4°C in 30% sucrose in PBS for dehydration. Once the organoids had completely sunk, they were transferred into embedding molds (Sigma-Aldrich), embedded in OCT compound (Thermo Fisher Scientific), and stored at -80°C. Cryostat sectioning was performed using a CM3050 S cryostat (Leica) to obtain 20 μm thick sections. For immunostaining, sections were washed five times with DPBS and blocked for 1 hour at room temperature in a blocking solution [1x PBS, 0.1% Triton X-100, 10% donkey serum (Merck), 2% BSA (MP Biomedicals), and 1 M glycine (Daejung)]. The sections were then incubated for 1 hour at room temperature with primary antibodies against DCX (Abcam) and nestin (Millipore). After washing five times with 0.1% Triton X-100 (Sigma-Aldrich) in PBS, the sections were then incubated with fluorescently conjugated secondary antibodies (Jackson ImmunoResearch) diluted in the blocking solution along with Hoechst 33342 (Invitrogen) for an additional 1 hour at room temperature. After washing five times with 0.1% Triton X-100 in PBS, the cover glass was mounted on slide glass. Images were acquired using the LSM 800 confocal microscope (Zeiss).

For analysis of the organoid surface region, the area corresponding to 20% of the total region, approximately 100∼180 μm inward from the surface was analyzed using ImageJ.

Immunoblotting

Cerebral organoids were harvested and lysed using RIPA buffer [50 mM Tris (Duchefa Biochemie), pH 8.0, 150 mM NaCl (Sigma-Aldrich), 1% NP-40 (Sigma-Aldrich), 0.5% sodium deoxycholate (Sigma-Aldrich), 0.1% SDS(Sigma-Aldrich)] containing protease and phosphatase inhibitors. Protein concentrations were measured using a BSA assay (Bio-Rad). An equal amount of protein for each sample was loaded and separated by SDS-PAGE and transferred to PVDF membranes. Then the membranes were incubated with blocking buffer [1x PBS, 0.1% Tween-20 (Promega), 5% skim milk powder (MB cell)] for 1 hour at room temperature. After blocking, the membranes were incubated overnight at 4°C with the following primary antibodies: SOX2 (Abcam), DCX (Abcam), TUJ1 (BioLegend), and GAPDH (Santa Cruz). Then, the membranes were washed three times with PBS and incubated with secondary antibodies for 1 hour at room temperature.

Flow cytometry analysis from cerebral organoids

One-month-old cerebral organoids were washed with DPBS and then dissociated using the Papain Dissociation System (Worthington Biochemical) following the manufacturer's instructions. The resulting single-cell suspension was fixed with 4% PFA for 15 minutes at room temperature and subsequently blocked for 1 hour in PBS containing 2% BSA and 0.1% Triton X-100. After blocking, the cells were incubated for 2 hours at 4°C with primary antibodies: a nestin PE-conjugated antibody (R&D Systems) and an antibody against DCX. Following three washes with 0.1% Triton X-100 in PBS, cells were stained with an Alexa Fluor 488-conjugated secondary antibody against DCX for 1 hour at room temperature. After another three washes with 0.1% Triton X-100 in PBS, the cells were resuspended in PBS and analyzed for nestin-positive and DCX-positive populations using FACS.

Immunocytochemistry

To conduct immunocytochemistry experiments, cells were washed three times with DPBS and fixed with 4% PFA solution for 10 minutes at room temperature. After fixation, cells were washed three times with DPBS and incubated with a blocking solution for 1 hour at room temperature. The cells were then incubated overnight at 4°C with the following primary antibodies: DCX, nestin, cleaved caspase 3 (Cell Signaling Technology), and Anti-phospho-Histone H2A.X (Millipore). After washing three times with 0.1% Triton X-100 in PBS, the cells were then incubated with fluorescently conjugated secondary antibodies diluted in blocking solution and Hoechst 33342 for 1 hour at room temperature. After washing three times with 0.1% Triton X-100 in PBS, the coverslips were mounted on slide glasses. Images were obtained with the LSM 800 confocal microscope and analyzed with ImageJ.

Seahorse extracellular analysis

XF plates were prepared by coating with Matrigel, and cells were seeded into the plates, excluding the blank wells. After maintaining NPCs and differentiating them into neurons for one week, the ATP rate assay was conducted. The day prior to the assay, the Agilent Seahorse XFp Analyzer was turned on to prewarm overnight. A sensor cartridge was hydrated and the subdivided calibrant was incubated at 37°C in a non-CO_2 incubator overnight. On the day of the assay, the cartridge, assay medium (composed of 10 mM D-glucose, 2 mM L-Glutamine, 1 mM Sodium Pyruvate in XF DMEM, adjusted to pH 7.4 at 37°C), and the Seahorse XFp cell culture miniplate were prepared. Cells were carefully washed twice with the assay medium, and finally 50 μL of the medium was added to each well. Stock compounds were then prepared (to achieve final concentrations of 1.5 μM oligomycin and 0.5 μM rotenone plus antimycin A) and loaded into the sensor cartridge. The experimental template was uploaded to the Seahorse analyzer, which then detected the real-time data. The results were subsequently analyzed using Seahorse Wave Software (Agilent).

EdU staining

EdU staining was performed using the Click-iT EdU Alexa Fluor 594 Imaging Kit (Invitrogen) according to the manufacturer's instructions. In brief, NPCs were incubated with EdU (1 μM) at 37°C for 4 hours, 10 hours, 16 hours, or 24 hours. NPCs were then washed three times with DPBS and fixed with 4% PFA solution for 10 minutes at room temperature. After washing the NPCs three times with 0.1% Triton X-100 in PBS, they were incubated with EdU reaction cocktail for 30 minutes at room temperature. The NPCs were then washed with 3% BSA in PBS and mounted on slide glasses for imaging.

MitoSOX staining and Fluorescence-activated Cell Sorting (FACS)

NPCs were dissociated using Accutase, counted with the Countess II (Invitrogen), and distributed at a density of 4×10^6 cells per 1 ml in neural induction media supplemented with 20 ng/ml FGF. Subsequently, 1 μl of 5 mM MitoSOX (Invitrogen) and 2 μl of Live-or-Dye (Biotium) were added to suspended cells. The cells were then incubated at 37°C for 20 minutes on a ThermoMixer C (Eppendorf) at 500 rpm, protected from light. After staining, the cells were washed three times with DPBS and strained using a 35 μm cell strainer. The stained cells were then sorted by FACS, selecting Live-or-Dye negative and MitoSOX positive cells.

Transcriptomic analysis

Extracted total RNA was subject to RNA-seq library preparation. Libraries were pooled for sequencing using Illumina NGS platform. The raw fastq data were aligned to human hg38 assembly using STAR 2.4.0 RNA-seq aligner.[40] Gene raw counts were generated from the mapped data using featureCounts tool.[41] Gene raw count matrix was processed by DESeq2 1.26.0 package[42] for differential expression analysis using negative binomial model. To explore the gene ontology of DEGs for the 'biological process,' the ToppGene Suite[43] or SynGO was used. To determine the overlap of neurogenesis cell markers with the human database, Fisher's exact test was performed to check the statistical significance of gene overlap of cell-type specific genes identified in GSE104276[20] with up and down-regulated gene lists identified from our RNA-seq data and presented in heatmap. Pseudotime trajectory analysis using GSE104276 database and our RNA-seq data was performed with Monocle2.[46] In brief, the expression matrix of 1540 single cells subject to NPC neuroglia pseudotime analysis in the original paper was collected and combined with the count matrix of in-house bulk RNA-seq data for cross-sample normalization using DESeq2 package. Genes with a minimal expression value of 0.1 were kept for trajectory analysis. 1180 Cell-type specific markers identified in the original paper were used as ordering genes for setOrderingFilter function. Dimension reduction was performed using the DDRTree method. WGCNA[47] was applied to explore gene co-expression pattern. Briefly, genes with average FPKM values greater than 0.1 were selected for calculating a set of soft-thresholding powers for signed network construction. A power value with SFT.R.sq > 0.9 (approximately scale-free) was chosen to compute adjacency matrix for a signed co-expression network. The topological overlap matrix (TOM) was then calculated, and average linkage hierarchical clustering was used to group genes based on their topological overlap. A dynamic tree-cutting method was used (minClusterSize = 100 and cutHeight = 0.999) to create gene co-expression modules and the results were visualized in a dendrogram. For module-trait correlation analysis, module eigengene values were correlated with sample trait values to calculate Pearson's correlation value and statistical significance as instructed in WGCNA tutorials and presented in a heatmap. Gene connectivity within each individual module was exported to VisANT for network visualization. Only the top 30 hub genes with the highest connectivity scores were presented in the network. To explore the gene ontology for the 'biological process,' the ToppGene Suite was used.

Transcription factor binding motif enrichment

Transcription factor binding motifs in promoter regions of genes in the turquoise module were identified using HOMER[44] with the settings findMotifs.pl <goi.txt> human <output_path> -bg <bg.txt>. Promoter regions of all genes included in the differential analysis were provided to HOMER as background regions. Known HOMER motifs were selected using HOMER calculated q-values (Benjamini) $\leq$ 0.05 and fold enrichment $\geq$ 2 (% motif present in target regions / % motif in background regions). HOMER motifs were converted to meme format and matched to putative transcription factors using Tomtom[48] and the HOCOMOCO v12 database for known transcription factors using tomtom motif.meme H12CORE_meme_format.meme -o <output_path>. Matched transcription factors were selected with q-value $\leq$ 0.0001 and were assessed for differential gene expression across APPswe NPC (versus control), high-ROS NPC (versus low-ROS NPC), high-ROS neuron (versus low-ROS neuron). Promoter regions with TFE3 binding sites were extracted using HOMER annotatePeaks.pl tss hg38 -size -300,50 -list <goi.txt> -m <TFE3.motif>. Gene ontology pathways for TFE3 gene promoters were assessed using PANTHER[45] using all genes included in the differential analysis as background. Repeated terms with the same content were excluded.

QUANTIFICATION AND STATISTICAL ANALYSIS

Prism 10 (GraphPad) was used for statistical analysis. Unpaired Student's t-test or one-way ANOVA test with Dunnett's post hoc analysis was used. The asterisks are defined in each relevant figure legends, together with the name of the statistical test.